Low-noise InGaAs/InP SPAD with photon detection efficiency exceeding 50% at 1550 nm

Fabio Telesca, Fabio Signorelli, Lorenzo Finazzi, Enrico Conca, Alberto Tosi
Dipartimento di Elettronica, Informazione e Bioingegneria, Politecnico di Milano, Italy
fabio.telesca@polimi.it

Abstract - *We designed a high-performance InGaAs/InP single-photon avalanche diode (SPAD) optimized for fiber-based quantum optics applications. Photon detection efficiency (PDE) was enhanced thanks to a thicker InGaAs absorption layer, while dark count rate (DCR) was kept under control through careful adjustment of the double zinc diffusion and the addition of a contacted guard ring structure. Our SPAD exhibits a PDE of 56% at 1310 nm and 51% at 1550 nm, with a DCR of 20 kcps, and a timing jitter of ~70 ps (FWHM) at 225 K. At lower excess bias (V_{EX}), a PDE of 40% at 1310 nm and 37% at 1550 nm is achieved with a dark count rate of just 3 kcps and a timing jitter of ~ 100 ps (FWHM). When wire-bonded to a custom integrated circuit, the afterpulsing probability is ~ 8%, with a gating frequency of 1 MHz and a hold-off time of 1 µs (max count rate is 1 Mcps) at 225 K and V_{EX} = 5 V and dropped below 3% at 10 µs hold-off.*

INTRODUCTION

InGaAs/InP single-photon avalanche diodes (SPADs) are the detectors of choice for many applications in the short-wavelength infrared range (SWIR), from light detection and ranging (LiDAR) [1] to quantum technology [2-4], thanks to their many advantages in terms of compactness, cost and ease of use. However, especially for quantum optics applications, their PDE needs to be further increased.

We designed a new InGaAs/InP SPAD with enhanced PDE (> 50%) at telecom wavelengths, showing low noise and moderate afterpulsing probability.

DEVICE STRUCTURE

Our InGaAs/InP SPAD is front-illuminated and features an active area diameter of 10 µm, optimized for being pigtailed to a single-mode optical fiber. The separate absorption, grading, charge and multiplication heterostructure from our previous generation [5] SPAD (Figure 1) was improved by doubling the absorption layer thickness, to increase the absorption of impinging SWIR photons. This change required a complete redesign of the other SPAD parameters: we tailored the double zinc diffusion profile and the charge layer, to limit the electric field and reduce noise, through better uniformity of avalanche triggering probability inside the active area (TCAD simulation results in Figure 3). Moreover, we added a guard ring (GR), equipped with its own metal contact (Figure 2): it can be biased independently of the main p-n junction, to contrast charge persistence [6] by sinking holes from the peripheral region of the SPAD before they reach the active area, and to improve active area uniformity by further mitigating edge breakdown.

EXPERIMENTAL RESULTS

DCR –The effect of guard ring bias on DCR is shown in Figure 4. DCR was measured in gated mode, with a fixed gate period of 100 µs, to rule out afterpulsing. As the GR junction is more reverse-biased ($\Delta V_{GR\text{-}Anode}$ is decreased), the electric field beneath the GR increases, and so does its positive effect on charge persistence and DCR. However, if a too high $\Delta V_{GR\text{-}A}$ is applied, breakdown occurs beneath the guard ring, which is undesirable. With the optimal $\Delta V_{GR\text{-}A}$, we acquired DCR measurements for different temperatures and excess bias voltages (Figure 5): we measured a DCR of just few kcps at the typical operating temperature of 225 K. At 200 K, DCR increases when V_{EX} is more than 7 V due to the residual charge persistence effect, while at 175 K DCR decreases again despite charge persistence is stronger, since thermal carrier generation is greatly reduced. All the measurements reported in the following were acquired with the optimal $\Delta V_{GR\text{-}A}$ that reduces the DCR.

PDE – We measured PDE at 1310 and 1550 by focusing a CW laser inside the active area of the detector with a spot size of ~5 µm (similar size of a pigtailing system from a SMF28 optical fiber). PDE is 51% at 1550 nm and 56% at 1310 nm, with a DCR below 20 kcps (see Figure 7). At lower V_{EX}, PDE is 37% and 41% at 1550 nm and 1310 nm, respectively, with a DCR of 3 kcps. PDE maps at 1550 nm are shown in Figure 6: as the excess bias is increased, uniformity of the PDE is improved, since the avalanche triggering probability tends to saturate at high electric field. The same trend holds at all wavelengths.

AFTERPULSING - The afterpulsing probability (APP) was measured with the SPAD wire-bonded to a custom front-end integrated circuit [5], which senses and actively quenches the avalanche in ~ 1 ns to limit APP. The integrated circuit is able to gate and quench up to V_{EX} = 5 V. Figure 8 and Figure 9 show the afterpulsing probability, calculated with TCCC method [7], as a function of hold-off time at T = 225 K. Afterpulsing becomes negligible (i.e., < 0.01%) if the hold-off time is longer than 50 µs, it is just 0.3% with 20 µs hold-off. The detector can be operated up to 1 Mcps (i.e., 1 µs hold-off time) with an APP of ~ 8%.

TIMING JITTER – When stimulated by a 1550 nm pulsed laser with 18 ps pulse width (FWHM) focused inside the SPAD active area, the SPAD under test features a narrow timing jitter, with a FWHM ranging from 72 ps at V_{EX} = 11 V to 319 ps at V_{EX} = 3 V (see Figure 10).

CONCLUSIONS

We presented a low-noise InGaAs/InP SPAD with enhanced PDE, thanks to a thicker absorption layer, a re-designed double zinc diffusion, a finely tuned charge layer and an additional biased guard ring. PDE is 51% at 1550 nm and 56% at 1310 nm, with 20 kpcs DCR at a temperature of 225 K, and a narrow timing jitter of ~ 70 ps (FWHM). A dedicated integrated circuit was employed to measure APP at 225 K, which resulted as low as few percent. Table I compares the performance of the detector here presented with other similar works: our SPAD features very high PDE together with low DCR and low timing jitter.

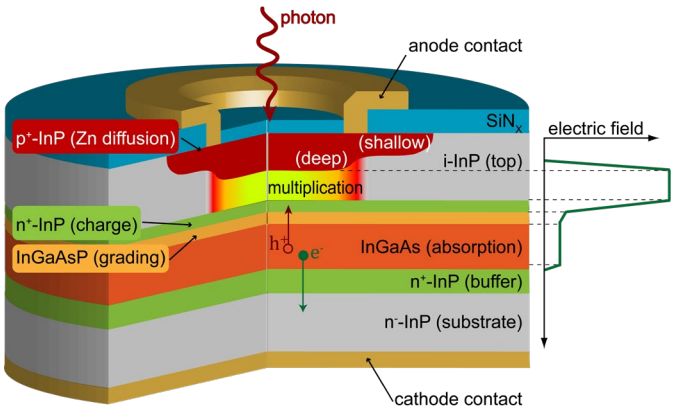

Figure 1: Cross-section of the front-illuminated InGaAs/InP SPAD here presented. A qualitative plot of the electric field along the vertical direction at the detector center is also reported on the right.

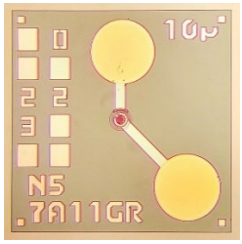

Figure 2: Micrograph of the fabricated InGaAs/InP SPAD. Bottom right pad: SPAD anode. Top pad: GR contact. The cathode is contacted from the backside

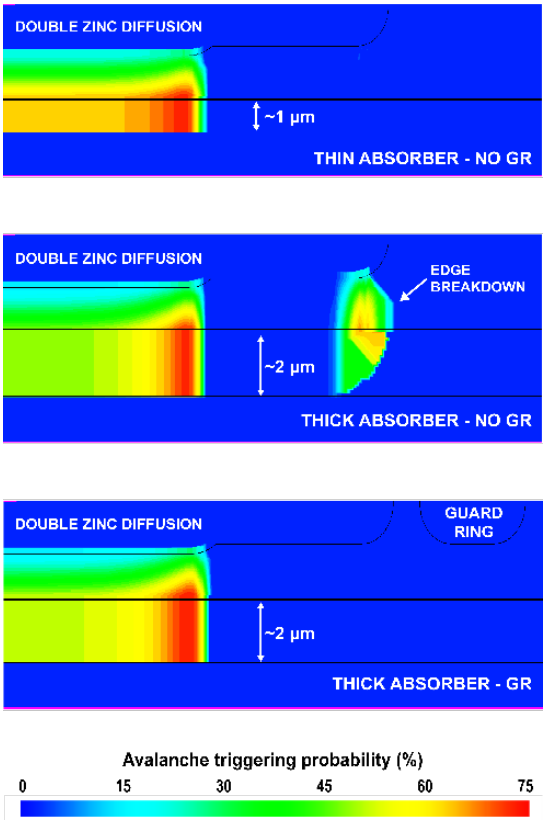

Figure 3: Examples of avalanche triggering probability TCAD simulations for InGaAs/InP SPADs with thin [5] and thick absorber (only half of the detector is represented). A guard ring is added in the thicker structure to avoid edge breakdown.

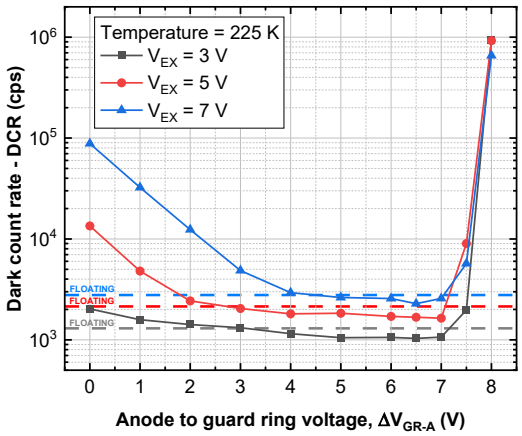

Figure 4: Dark count rate as a function of the bias voltage ΔV_{GR-A} between the guard ring and SPAD anode, at different excess bias voltages. DCR values when the guard ring is left floating are reported as dashed horizontal lines.

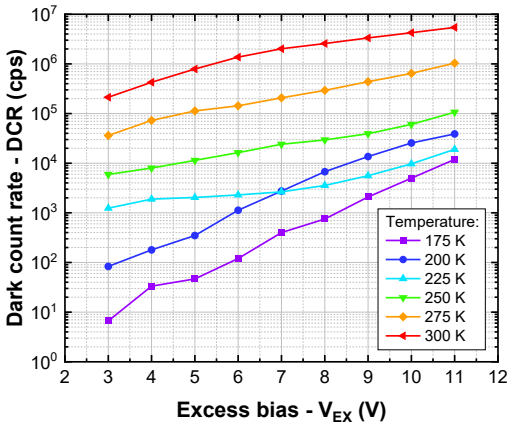

Figure 5: Dark count rate as a function of the excess bias voltage at different operating temperatures. The GR was biased to the optimal condition to minimize DCR.

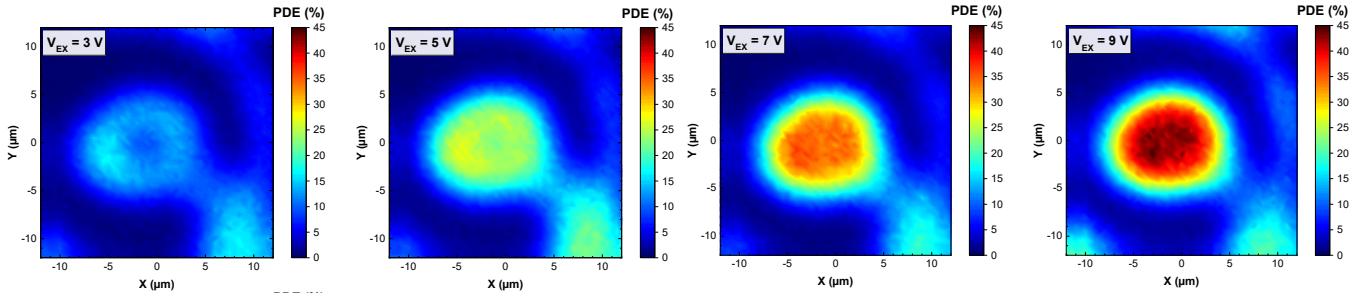

Figure 6: 2D maps of photon detection efficiency at different excess bias voltages. The scale is the same for all the maps. The images show minor distortions due to positioning issues when the laser spot is scanned by means of a xyz motorized micro-positioning system.

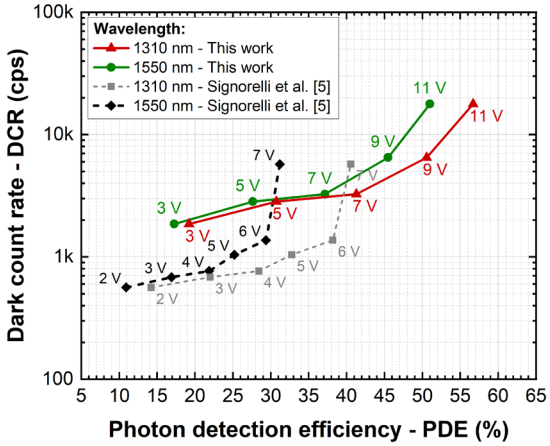

Figure 7: Photon detection efficiency (at 1310 nm and 1550 nm) and dark count rate at different excess bias voltages, for both the thick SPAD here presented and the thin one described in [5].

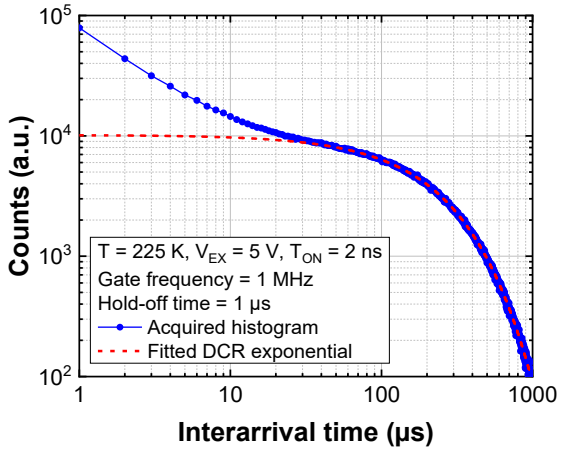

Figure 8: Example of acquired inter-time histogram. The difference between the acquired curve and the fitted exponential curve (corresponding to the distribution of primary DCR) is due to afterpulsing.

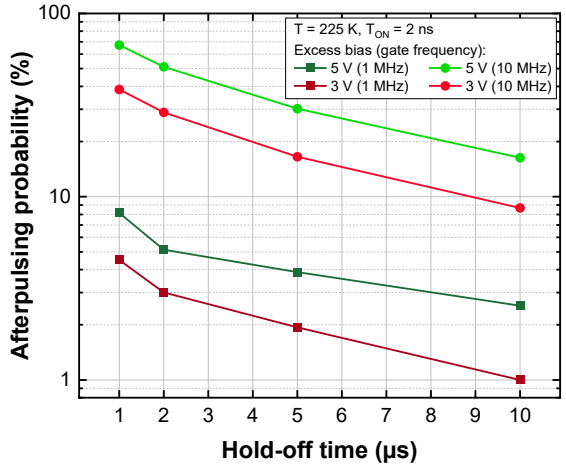

Figure 9: Afterpulsing probability as a function of hold-off time at various V_{EX} and gating frequencies.

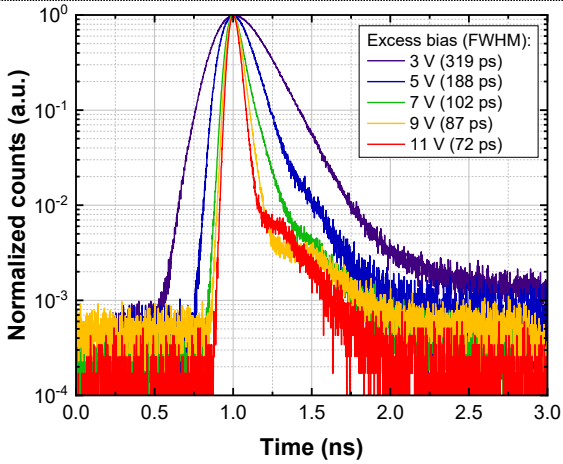

Figure 10: Instrument response function (at different excess bias voltages) to a pulsed laser (18 ps FWHM) at 1550 nm, focused inside the active area.

TABLE 1

PERFORMANCE OF STATE-OF-THE-ART InGaAs/InP SPADs

Reference	Active area diameter (∂m)	Temperature (K)	DCR (cps) @ PDE (%)	APP (%) @ HO time (ns)[a]	Timing jitter (ps) @ PDE (%)
This work	**10**	**225**	**1.9 k – 18 k @ 17.3 – 51**	**4.5 – 8.1 @ 1000**	**319 – 72 @ 17.3 – 51**
Signorelli *et al.* [5]	*10*	225	560 - 1370 @ 11 - 30	1.4 - 4.4 @ 1000	225 - 84 @ 11 - 30
Baek *et al.* [8]	16	233	100 - 1000[b] @ 10 - 31	2 - 7[c]	N.A.
		293	2 k - 20 k[b] @ 10 - 31	1 - 2.5[c]	
Fang *et al.* [9]	25	233	260 - 2.5 k @ 7 - 37	4.8 - 12.5 @ < 0.8[c]	N.A.
		253	900 - 21.6 k @ 7.5 - 46	1.4 - 12.6 @ < 0.8[c]	
Tamura *et al.* [10]	9	233	22.2 k - 111.1 k[d] @ 10 - 48[e]	61.5 - 90	450 – 400 @ 10 - 50
He *et al.* [11]	20	247	1000 - 43.8k @ 8 – 55.4	N.A.	N.A.
Zhang *et al.* [12]	12	233	127 – 1000 @ 10 - 40	3 – 22 @ 20[f]	N.A.

[a] APP = afterpulsing probability, HO = hold-off, only reported when available. [b] Computed from dark count probability per gate, with gate frequency = 10 MHz, gate width = 2 ns. [c] Changes with gate signal amplitude. [d] DCR of the single pixel computed as 1/9th of the DCR of a 3×3 array. [e] Afterpulse probability not subtracted. [f] gate width = 1 ns.

REFERENCES

[1] X. Jiang et al., "InGaAsP/InP Geiger-mode APD-based LiDAR", doi: 10.1117/12.2322757.
[2] X. Jiang et al., "InP-based single-photon detectors and Geiger-mode APD arrays for quantum communications applications", doi: 10.1109/JSTQE.2014.2358685.
[3] N. Gisin and R. Thew, "Quantum communication", Nat. Photon., vol.1, no. 3, pp. 165–171, Mar. 2007.
[4] T. D. Ladd et al., "Quantum computers" Nature, vol. 464, no. 7285. Nature Publishing Group, pp. 45–53, Mar-2010.
[5] F. Signorelli et al., "Low-Noise InGaAs/InP Single-Photon Avalanche Diodes for Fiber-Based and Free-Space Applications", doi: 10.1109/JSTQE.2021.3104962.
[6] N. Calandri, et al., "Charge Persistence in InGaAs/InP Single-Photon Avalanche Diodes", doi: 10.1109/JQE.2016.2526608.
[7] S. Cova, et al., "Trapping Phenomena in Avalanche Photodiodes on Nanosecond Scale", doi: 10.1109/55.116955.
[8] S. H. Baek, et al., "Room temperature quantum key distribution characteristics of low-noise InGaAs/InP single-photon avalanche diode", doi: 10.1007/s40042-021-00111-4.
[9] Y. Q. Fang et al., "InGaAs/InP single-photon detectors with 60% detection efficiency at 1550 nm", doi: 10.1063/5.0014123.
[10] Y. Tamura et al., "Development of InGaAs MPPC for NIR photon counting applications", Proc. SPIE, Optical Components and Materials XV, Feb. 2018, p. 35.
[11] T. He et al., "High photon detection efficiency InGaAs/InP single photon avalanche diode at 250 K", doi: 10.1088/1674-4926/43/10/102301.
[12] B. Zhang et al., "High Performance InGaAs/InP Single-Photon Avalanche Diode Using DBR-Metal Reflector and Backside Micro-Lens", doi: 10.1109/JLT.2022.3153455.